2

Voltage-Dependent Gating of Ion Channels

Baron Chanda and Sandipan Chowdhury

CONTENTS

2.1 Introduction

Electrical signaling is well suited for cell–cell communication and fast processing of complex information in an ever-changing environment. Unlike purely chemical second-messenger pathways, electrical signaling is confined to the plane of a membrane and can travel long distances rapidly. These signaling pathways have been found in all three kingdoms of life and the molecular parallels between distantly related species is quite remarkable. Even in the lowly bacterial cells, "action potential" like electrical signals have been shown to underpin social communication during formation of drug-resistant biofilms (Humphries et al. 2017).

To sense and respond to changes in membrane potential, proteins including ion channels must have charges or dipoles positioned in the transmembrane regions where the electric field is extremely large. The potential gradient within the bilayer can be as high as 10^6 V/m. In a typical voltage-sensitive ion channel, movement of the sensing charges in response to a change in the electric field is coupled to conformational changes in the pore domain, which serves as a gated conduit for the flow of ions (Bezanilla 2000).

DOI: 10.1201/9781003096214-3

The channels in the voltage-gated ion channel (VGIC) superfamily can be very sensitive to membrane potential. Some of these channels increase their activity by many orders of magnitude in response to a few millivolts change in membrane potential. Thus, channels in this family include some of the most tightly regulated allosteric molecules known to date. The overall architecture of members of this superfamily is conserved. Each functional channel has four specialized voltage-sensing domains (VSDs), which surround a central pore domain (Long, Campbell, and Mackinnon 2005a). Each VSD consists of four transmembrane helices where the fourth helical segment contains positively charged residues at every third position. These VSD charges sense and respond to the membrane potential and are the primary drivers of downstream conformational changes that ultimately determine the activity of these channels. Although this architecture is broadly conserved, we should note that some channels like the voltage-gated proton channels (Hv1) lack a specialized pore domain (Sasaki, Takagi, and Okamura 2006; Ramsey et al. 2006) (Figure 2.1).

Since the pioneering studies by Bernstein, Cole, Hodgkin, Huxley and others, voltage-sensitive conductances have been extensively studied because of their primary role in electrical excitability in a variety of cell types which include nerves, muscles, cardiac cells

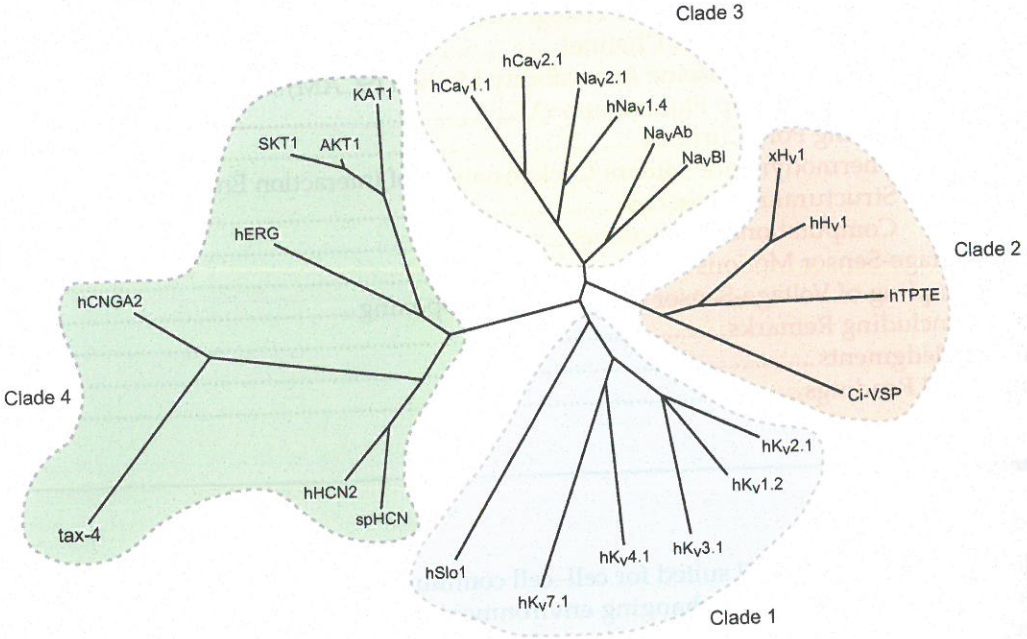

FIGURE 2.1
Phylogenetic tree of voltage-gated ion channels. The cladogram shows the sequence diversity of 24 voltage-sensing domains (VSDs) from different members of the VGIC family, created from a multiple sequence alignment of the VSDs (obtained using MUSCLE). The phylogenetic tree calculation was performed using MATLAB 2012 (MathWorks) and BioNJ. Four distinct clades are directly observable. Clade 1 comprises the different voltage-gated potassium channels members of which form homotetrameric channels. Clade 2 comprises the voltage-sensor-only proteins (VSOPs) – the proton selective H_V channel (human and Xenopus) and the PTEN phosphatase domain containing VSOPs from *Ciona intestinalis* and its human orthologue (hTPTE). Clade 3 comprises the voltage-gated sodium and calcium channels from eukaryotes (which are heterotetrameric; $Na_V2.1$ represents the sodium channel from *Nematostella vectensis*) and prokaryotes (NavAb and NavBl). Clade 4 comprises members of the VGIC family containing a cyclic nucleotide binding domain at their C-termini. Members of this clade include the depolarization-activated hERG channels, hyperpolarization-activated channels from metazoans (hHCN2 and spHCN), the inwardly rectifying plant channels (SKT1, AKT1 and KAT1) and the very weakly voltage-sensitive CNG channels (human and *C. elegans* orthologues).

among others (Bernstein 1902, 1912; Cole and Curtis 1939; Hodgkin and Huxley 1952a, 1952b, 1952c, 1952d, 1952e; Hodgkin and Rushton 1946). Voltage-dependent cation channels, which include the K^+, Na^+ and Ca^{++} channels, are responsible for generation of electrical impulses in many cell types. The influx of Ca^{++} ions through voltage-dependent Ca^{++} channels can also act as a second messenger that initiates various processes such as muscle contraction, exocytosis and cell secretion, proliferation, and migration (Hagiwara 1966; Hagiwara and Nakajima 1966).

Much of our current understanding of the mechanisms of voltage-sensing comes from studies on exemplar VGICs, but it is worth noting that many channels lacking VSD also exhibit voltage-dependent activity. For instance, Kir channels are inwardly rectifying due to voltage-dependent pore block by divalent cations (Lopatin, Makhina, and Nichols 1994). Similarly, K2P channels, which are also lacking in VSD, exhibit strong outward rectification (Schewe et al. 2016). These noncanonical mechanisms will be discussed in detail elsewhere.

2.2 Basic Principles of Voltage Sensing

For more than half a century, voltage-clamp experiments have been the bedrock of electrophysiological methods to analyze biophysical properties of voltage-gated ion channels. In this technique, we measure the amount of current flowing through the membrane expressing channels in response to step changes in potential. From their time-dependent current responses, we can deduce their rates of opening and closing and the fraction of open channels when a new equilibrium is established. The analysis of voltage dependence of open probabilities provides a measure of the relative stability of the open versus closed state of the channel. In the next few sections, we will discuss the quantitative framework for describing the time- and voltage-dependent properties of channel activity and derive fundamental insights into the mechanisms of voltage activation.

2.2.1 Two-State Model of Voltage Gating

From a physical perspective, this voltage-dependent change in channel open probability can be treated as a two-state process wherein the channel exists either in the closed or open state, and voltage biases the equilibrium toward one state or the other.

$$C \rightleftharpoons O$$

Analogous to a chemical reaction, the equilibrium constant for this system is

$$K(V) = \exp\{-\Delta G(V)/RT\} \tag{2.1}$$

where $\Delta G(V)$ is the voltage-dependent energy difference between the two states (Figure 2.2A). In channels that open in response to depolarization, the equilibrium is biased toward the closed state at resting membrane potentials (~–90 mV) and a depolarizing shift in this potential favors channel opening. Furthermore, the energy difference between the two states at a particular voltage is determined by the chemical energy difference between the two states (ΔG_C) and electrical work that is done on this system $\Delta G(V)$:

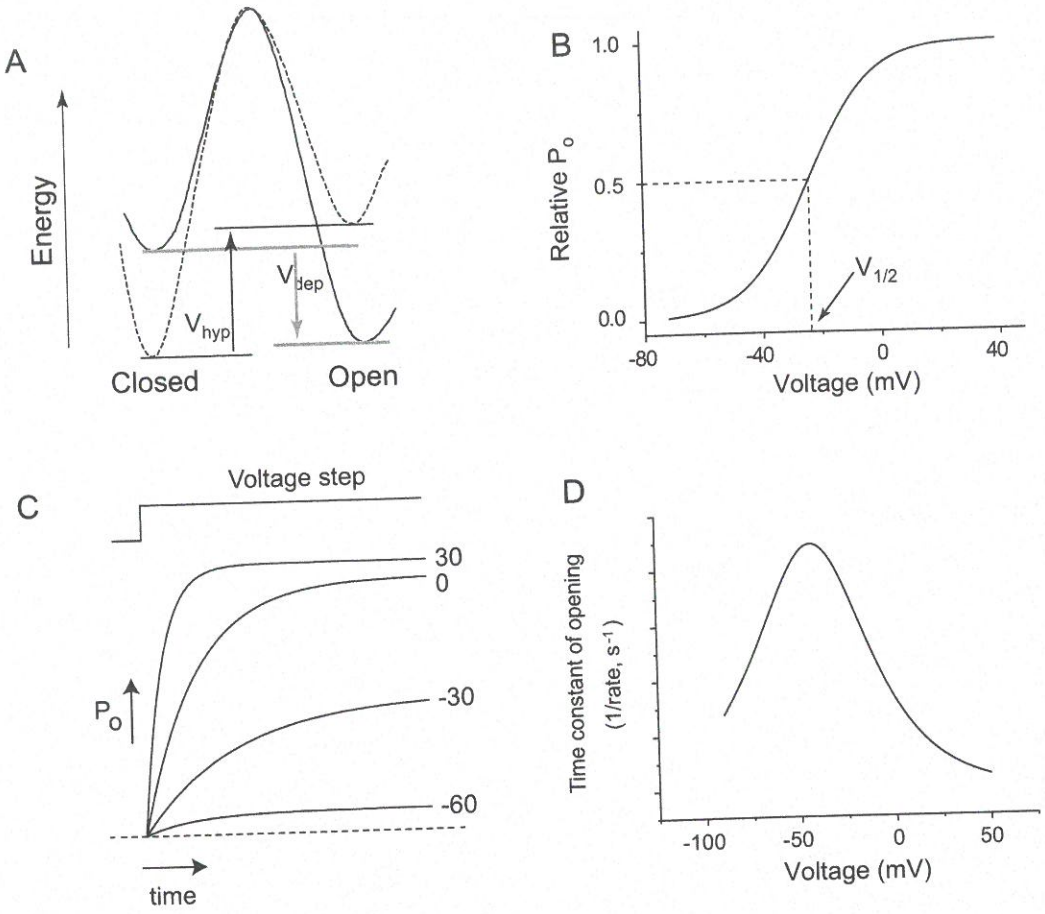

FIGURE 2.2
Steady-state and equilibrium properties for a binary gating model. (A) Energy profile diagram of a closed to open transition for a VGIC. At a hyperpolarizing voltage, V_{hyp} (dotted profile), the closed state is energetically more favorable than the open state. At a depolarizing voltage, V_{dep} (solid profile), the open state is more stable than the closed state. The net energy difference between the closed states at V_{hyp} and V_{dep} are indicated using arrows. (B) The open probability versus voltage curve for a channel that undergoes a binary transition between a closed and an open state. The voltage at which half the channels are open is indicated by $V_{1/2}$. (C) Time-dependent increase in open channel probability of a channel stimulated by voltage jumps to different depolarizing voltages from a constant hyperpolarizing voltage when channels are closed. (D) The time constant of channel opening at different voltages varies nonmonotonically.

$$\Delta G(V) = \Delta G_C - qFV \tag{2.2}$$

where ΔG_C governs the intrinsic conformational bias of the channel in the absence of imposed voltage and q (sometimes referred to as Δq) is the charge difference between the two states, F is Faraday constant, and V is the voltage difference between the inner and outer leaflets of the membrane. The key takeaway here is that a two-state process will be voltage-dependent, only if there is a charge movement associated with the transition.

We can learn about the energetics and kinetics of these processes from measurements of channel activity using voltage-clamp experiments. In a typical experiment, the relative

channel open probability is obtained at various voltages and is related to the voltage-dependent equilibrium constant by the following equation:

$$K(V) = \frac{P_O}{1 - P_O} \tag{2.3}$$

$$P_O(V) = \frac{1}{1 + \frac{1}{K(V)}} \tag{2.4}$$

By combining Equations 2.1 and 2.2,

$$K(V) = \exp\{-(\Delta G_C - qFV)/RT\} \tag{2.5}$$

Therefore,

$$P_O(V) = \frac{1}{1 + \exp\{(\Delta G_C - qFV)/RT\}} \tag{2.6}$$

At a particular voltage, ΔG_C will equal qFV and as a result P_O will become 0.5. Thus, we can reparameterize ΔG_C as $qFV_{1/2}$, where $V_{1/2}$ is the voltage at which P_O is 0.5. Thus Equation 2.6 can be rewritten as

$$P_O(V) = \frac{1}{1 + \exp\{qF(V_{1/2} - V)/RT\}} \tag{2.7}$$

The preceding equation is an S-shaped logistic function that is used to describe the open probability versus voltage (P_O–V) relationship for channel opening and is commonly known as the Boltzmann equation. It is noteworthy that, because of the reparameterization, $qFV_{1/2}$ represents the chemical free-energy difference between the closed and open state, and can be obtained by fitting an experimentally deduced P_O–V curve to the Boltzmann equation. A more negative value of $V_{1/2}$ implies that at zero voltage, the open state is intrinsically more stable than the closed state.

In addition to affecting the equilibrium occupancies of the open and closed states, voltage also alters the rates of channel opening and closing. From an Eyring rate theory perspective, channel opening and closing both encounter an activation energy barrier, but these must also be voltage sensitive. Accordingly, the voltage-dependent microscopic rates of channel opening and closing, k_O and k_C respectively, are expressed as

$$k_O = k_O^{\#} \exp(q_O FV) \tag{2.8a}$$

$$k_C = k_C^{\#} \exp(-q_C FV) \tag{2.8b}$$

where $k_O^{\#}$ and $k_C^{\#}$ reflect the respective rates in the absence of voltage (i.e. 0 mV). q_O accounts for the voltage dependence of k_O and can be interpreted as the charge that must move

between the closed state and the transition state. Similarly, q_C represents the charge that moves between the open state and the transition state during channel closing. The opposite signs of the exponents in Equations 2.8a and 2.8b are important since it indicates that when voltage is increased, channel opening becomes faster but channel closing becomes slower.

The time-dependent evolution of the open channel probability in response to a depolarization pulse can be expressed as

$$P_O(t) = P_O^{eq}.\left(1 - A.\exp\left\{-\left(k_O + k_C\right)t\right\}\right) \tag{2.9a}$$

In the preceding equation, P_O^{eq} is the equilibrium occupancy of the open state when channels reach a steady-state at the imposed depolarization. A is constant, which is determined by the initial occupancies of the open/closed states (in turn determined by voltage) prior to the depolarization pulse. The important point to note here is that the overall observed rate of channel opening is $\left(k_O + k_C\right)$. Thus, the time evolution of the open state is informed both by the rate constants of channel opening and closing. The reason behind this dependence is that the overall observed rates of channel opening (the time derivative of open channel probability) depend both on the unimolecular (or microscopic) rate constants as well as species fractions, i.e.,

$$\frac{dP_O}{dt} = k_O P_C - k_C P_O \tag{2.9b}$$

When voltage is increased, k_O increases (Equation 2.8a) and thus the positive term of Equation 2.9b increases too. However, with time, as more open channels populate, there will be more kinetic driving force for channel closing (due to the negative term in Equation 2.9b) and some of the channels which have opened, will now begin to close. The contribution of this negative term will depend on the magnitude of microscopic rate of channel closing, k_C. At a certain point in time, when the two terms become equal, the derivative will become zero and equilibrium is achieved. At strong depolarizing voltages, k_C will be negligibly small (Equation 2.8b) and thus the overall rate of channel opening will almost exclusively depend on k_O. The same principles apply to the kinetics of channel closing. This basic formalism can be applied to extract the rate constants of channel opening and closing from time evolution of channel activity in response to step potentials.

As is obvious by now, for a gating transition to be voltage sensitive, it must be associated with movement of charges (Armstrong 1981). Changes in the electric field are sensed either by translocating charges or via movement of dipoles within the membrane field. In the preceding two-state model, this sensing charge is the q, which is the net charge difference between the C and O state. The movement of "sensing" charges (also called gating charges) in response to changes in the electric field generates a current called gating currents. These currents are capacitive in nature because once the translocation of charge from one state to the other is complete, no further charge will be moved. Thermodynamics dictates that for a reversible reaction the total gating charge transported (obtained by integrating gating current over time) during a voltage pulse must be equal to the charge moved when the voltage is restored to its initial value. This equality of ON and OFF charge is a hallmark of gating currents for processes that are completely reversible.

To measure gating currents, it is necessary to eliminate ionic currents, which can be accomplished by either using specific blockers or by replacing the permeant ions. In the absence of ionic current, we are left with capacitive currents, which is due to buildup of charge in the lipid bilayer. The capacitive current, I_C, is the time derivative of the charge and can be written as

$$I_C = C\frac{dV}{dt} + V\frac{dC}{dt} \tag{2.10}$$

where C is the total capacitance and V is the voltage. The first term in Equation 2.10 corresponds to a fixed capacitor, which is due to the charging of the lipid bilayer, whereas the second term describes time-dependent changes in the capacitance of the membrane arising due to conformational transitions in the protein. The capacitance of the membrane itself is practically time invariant while the currents arising due to charge movements in the protein follow special kinetics governed by the energy-landscape of protein dynamics. The definition of capacitance is the ability to store charge and when there is a redistribution of charge in the membrane due to a gating transition, its capacity to store charge must also change. Since the proteins are sensitive to voltage over a relatively narrow, specified voltage-range the contribution of the second term to *Ic* will saturate at extreme potentials once the transition is completed and the charges within the protein reach their final position. In contrast, the first term will grow linearly with increasing potential as more free charges from the bath will keep accumulating across the lipid bilayer. This difference in the voltage dependence of the two components can be utilized to extract gating charges associated with voltage-sensing gating transitions (see Chapter 7 for more experimental details).

The time course of gating charge (Q) movement can be obtained by integrating the gating currents over time. For a two-state model, the time course of gating charge in response to a step depolarization corresponds to

$$Q(t) = N.q.P_O^{eq}\left(1 - A.\exp\left\{-\left(k_O + k_C\right)t\right\}\right) \tag{2.11}$$

where N is the number of channels and q is the gating charge per channel. P_O^{eq}, A and k_O, k_C have the same definitions as in Equation 2.9. Similarly, the voltage dependence of the gating charge in a two-state model is

$$Q(V) = \frac{N.q}{1 + \exp\left\{qF\left(V_{1/2} - V\right)/RT\right\}} \tag{2.12}$$

Except for a multiplicative factor, the expressions describing $Q(V)$ and $Q(t)$ are identical to $P_O(V)$ and $P_O(t)$, respectively. For a two-state model, the voltage dependence and time dependence of ionic currents and charge movement will be completely superposable. This is a hallmark of a two-state model but is rarely observed in practice. While gating behavior of most channels is more complicated and requires consideration of multiple transitions, the two-state model, nonetheless, serves as an excellent pedagogical tool to understand the behavior of a voltage-dependent process.

2.2.2 Multistate Models of Voltage Gating

In the 1950s, using the newly developed voltage-clamp technique, Hodgkin and Huxley (1952a, 1952b, 1952c, 1952d, 1952e) carried out a series of groundbreaking experiments that led to a detailed quantitative description of an action potential in the squid giant axon. They discovered that the sodium and potassium conductances in the squid giant axon are regulated independently and depend on membrane voltage rather than membrane currents. Furthermore, the time course of these currents did not correspond to monoexponential kinetics as expected in a simple two-state model (Equations 2.9 and 2.11). Nonetheless, the two-state model served as a starting point to develop their phenomenological model, which recapitulated the major features of excitability.

Their model, which is widely known as the Hodgkin–Huxley model, has two separate equations to describe the sodium and potassium conductances during an action potential. The potassium current (I_K) is represented as

$$I_K = n^4.g_K\left(V - V_K\right) \tag{2.13}$$

where g_K is the conductance of the conductance of the potassium channels, V is the applied voltage, V_K is the reversal potential and n refers to voltage-dependent probability of a gating particle to exist in either a permissive or nonpermissive state. Hence, the voltage dependence of this gating particle will be similar to the two-state particle shown in Equation 2.9, and we can rewrite the time dependence of the potassium current as

$$I_K(t) = n_\infty\left(1 - A.\exp\left\{-\left(k_O + k_C\right)t\right\}\right)^4 g_K\left(V - V_K\right) \tag{2.14}$$

The preceding equation is a powered exponential function that accounts for the steep voltage dependence and the pronounced lag phase observed in the potassium currents. As the power increases, the lag phase becomes prominent, and in the case of potassium currents, the time course was well fit to power of 4. Based on this empirical relationship, Hodgkin and Huxley presciently inferred that the increase in potassium conductance is regulated by four independent gating particles, all of which must move to a permissive state for ion flux. We now know that the potassium channel is a tetramer where a voltage-sensing domain in each subunit regulates the opening and closing of the channel.

Hodgkin and Huxley also described the time-dependent changes in sodium conductance along the same lines with four independent gating particles. However, to account for inactivation of sodium currents, they reassigned one of the probability terms to inactivation. In the following equation, m is probability of the three particles that contribute to channel opening to be in a permissive state and h is the probability of the inactivation particle to be in a nonpermissive state:

$$I_{Na} = m^3.h.g_{Na}\left(V - V_{Na}\right) \tag{2.15}$$

The kinetics of the inactivation particle is slower than those of the activation particles, which gives rise to the characteristic sodium channel transients. Remarkably, 50 years later, studies probing the structural dynamics of the voltage-sensing domains found that the voltage-dependent activation of the first three homologous domains of the sodium channel contributes to channel opening, whereas slow moving domain IV is a rate-limiting step for entry into an inactivated state (Chanda and Bezanilla 2002).

Some of the predictions of the Hodgkin–Huxley model were put to further tests when gating currents from sodium channels in the squid giant axon were first measured by Armstrong and Bezanilla (1973). To record these small transient currents, which till that point was viewed using oscilloscopes and chart recorders, they had to develop specialized electronics. They found that the sodium channel gating current is not monoexponential as predicted but instead exhibits a fast rising phase and a multiexponential decay. Furthermore, they found that the entry into inactivation slows the recovery of the gating charge when the voltage is returned to the original value, indicating that the activation and inactivation are coupled. These and other observations formed the basis of the coupled inactivation model, which postulates that the inactivation is not due to movement of the gating particle itself but follows upon channel opening (Armstrong 1992, 1981). This notion of inactivation as a linked reaction is widely accepted and has been validated by multiple lines of evidence.

Discovery of methods to make gigaohm resistance seals and the development of the patch-clamp technique by Neher and Sakmann ushered a new era whereupon it became possible to reliably record activity of single channels from native tissues with tremendous precision (Hamill et al. 1981). These measurements enabled the development of detailed kinetic models that were both parsimonious as well as mechanistically insightful. A detailed discussion of these models is provided in Chapter 7, but suffice it to say, these kinetic models of activation were further constrained by gating current recordings. The key feature of these models is that the pore opening and voltage sensing are distinct but linked processes. According to the model proposed by Zagotta, Hoshi and Aldrich for the Shaker potassium channel, the overall process of channel opening involves two sequential "voltage-sensing" transitions occurring independently in different subunits of the protein (Hoshi, Zagotta, and Aldrich 1994; Zagotta, Hoshi, and Aldrich 1994; Zagotta et al. 1994). Once all four voltage sensors are fully activated, a single concerted transition gates the channel open. The charge movement that accompanies the voltage-sensing steps are largely confined to a specialized voltage-sensing domain within each subunit of the protein and occur early in the activation pathway. The opening of the channel pore exhibits very little intrinsic voltage dependence and occurs late in the activation pathway (Figure 2.3).

The voltage dependence of channel gating depends on the amount of charge associated with voltage-dependent transitions, but how do we estimate the gating charge per channel (referred to as Q_{max})? In principle, all that is required is measurement of the maximum gating charge and an independent estimate of the number of channels in the same cell or patch of membrane. However, precisely estimating the number of active channels in a single cell is experimentally nontrivial. It was not until the 1990s that methods were developed and successfully implemented to calculate Q_{max}. Almers (1978) proposed a strategy that involves measuring the voltage-dependence of channel opening at voltages where channel opening probabilities are infrequent. This approach, referred to as the limiting slope analysis, allows researchers to calculate the charge per channel by simply using Po measurements. The slope at limiting voltages is calculated from a semilog plot of ln P_O versus V and can be described mathematically as

$$Q_{max} = \lim_{V \to -\infty} \frac{\partial \ln P_O}{\partial V} \tag{2.16}$$

Under these limiting conditions, the channel will spend most of its time in the first closed state, and to open it must traverse through all the intermediate states and hence the voltage

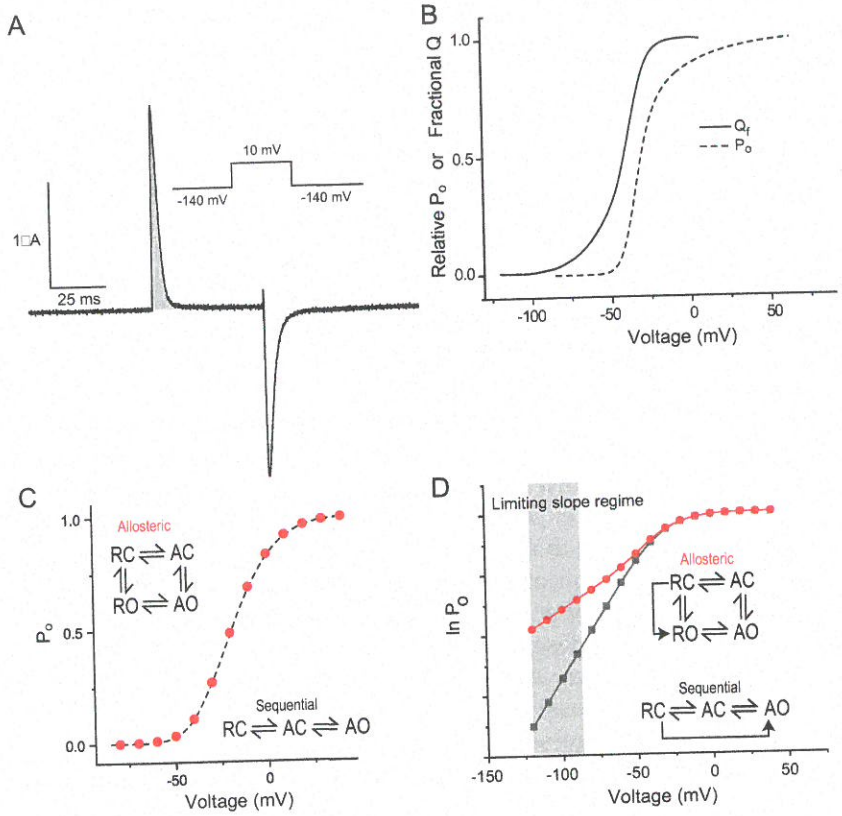

FIGURE 2.3
Gating charge movement in voltage-dependent ion channels. (A) An example of a gating current trace for the Shaker potassium channel (in the background of the W434F and inactivation-removing mutations) obtained in response to a depolarizing pulse. The shaded area represents the gating charge transferred during the depolarization. (B) Comparison of the normalized gating-charge displacement (Q_f) and relative open-probability curves for the Shaker potassium channel (inactivation removed mutant). (C and D) Open probability versus voltage relationships for channels which activate either allosterically (red dots) or strictly sequentially (dashed line). RC corresponds to resting voltage sensor and closed pore, RO corresponds to resting voltage sensor and open pore, AC corresponds to activated voltage sensor and closed pore, and AO corresponds to activated voltage sensor and open pore. In allosteric model, the channel consisting of a voltage sensor and pore can exist in all four possible states whereas in a strictly sequential scheme, some of the states such as RO are forbidden. Note that P_O versus V relationships (C) will appear identical, but the differences between the two models will become evident in $\ln P_O$ versus V plots (D). The limiting slope of the $\ln P_O$ versus V curves, measured in the shaded voltage range, correspond to the charge movement between the states indicated by the arrows. In the allosteric model, the limiting slope represents the charge moved between the RC and RO states, whereas in the sequential model, the limiting slope equals to the charge moved between the RC and AO states, which corresponds to the total gating charge associated with channel activation.

dependence of opening at these voltages reflects the sum total of all voltage-dependent transitions in the gating pathway. The underlying premise is that the channel activation is fully sequential and that the voltage sensor must always activate before the pore can open. However, in an allosteric scheme, where pore openings can occur even in absence of voltage-sensor activation (albeit with very low probability), the limiting slope method cannot be applied to calculate charge per channel.

2.2.3 Model-Free Methods for Estimating Free Energy of Channel Gating

The gating models described until now not only provide us a quantitative description of the time- and voltage-dependent behavior of channel activity but can also give mechanistic insights into the structural features. More sophisticated and structurally detailed models have been built since then by using orthogonal information from voltage-clamp fluorometry and above all by solving high-resolution structures of voltage-gated channels in various conformations. While the structures of the channel in various conformations are visually satisfying and provide a physical view of channel gating, they cannot be used to directly make quantitative predictions. Experimentally, the effects of mutations or perturbations can be manifested both in terms of equilibrium and kinetic properties. As a first approximation, it is fair to assume that interactions at equilibrium determine the structures of macromolecules, and changes in these interactions underlie conformational rearrangements that ultimately dictate function. In this section, we will review model-agnostic methods to estimate the free energy of channel gating and how these enable estimates of site-specific interactions.

Let us begin by considering the Zagotta–Hoshi–Aldrich model for voltage-dependent gating:

$$(R_1 \underset{}{\overset{K_1}{\rightleftharpoons}} R_2 \underset{}{\overset{K_2}{\rightleftharpoons}} C)_4 \underset{}{\overset{L}{\rightleftharpoons}} O$$

K_1, K_2 and L indicate the voltage-independent components of the equilibrium constants for each of the transitions. The net free energy of activation in this case is

$$\Delta G_C = -RT \ln\left\{\left(K_1 K_2\right)^4 L\right\} \tag{2.17}$$

In principle, it is not necessary to develop detailed kinetic models to estimate the net free energy of activation. We should also point out that these kinetic models have been developed for only a limited set of exemplar ion channels but are missing for the vast majority of the channels. A more direct approach to obtain G_c exploits an important thermodynamic principle that the free-energy change in a system will be equal to the work done on the system by the external force under reversible conditions (Chowdhury and Chanda 2012). The work done, in turn, depends on the external force and its conjugate displacement. For instance, in the case of mechanical work on an ion channel, the external force is surface tension or pressure whose conjugate displacements are surface area or volume expansions. In a similar way, when the work done is electrical in nature, the external force is voltage and its conjugate displacement is charge. Thus, for voltage-dependent ion channels, the free-energy change, G, can be estimated from the QV curve. Specifically, G is given by the integral of the QV curve (Figure. **2.4**a):

$$\Delta G = \int_{-\infty}^{\infty} QdV \tag{2.18}$$

Integration of this equation by parts allows us to separate this G into two components:

$$\Delta G = \lim_{V \to -\infty} Q_{max} FV - \int_0^{Q_{max}} VdQ \tag{2.19}$$

The first ($Q_{max}FV$) is the electrical component (where Q_{max} is the maximum number of gating charges transferred during channel activation); the second component, which is the

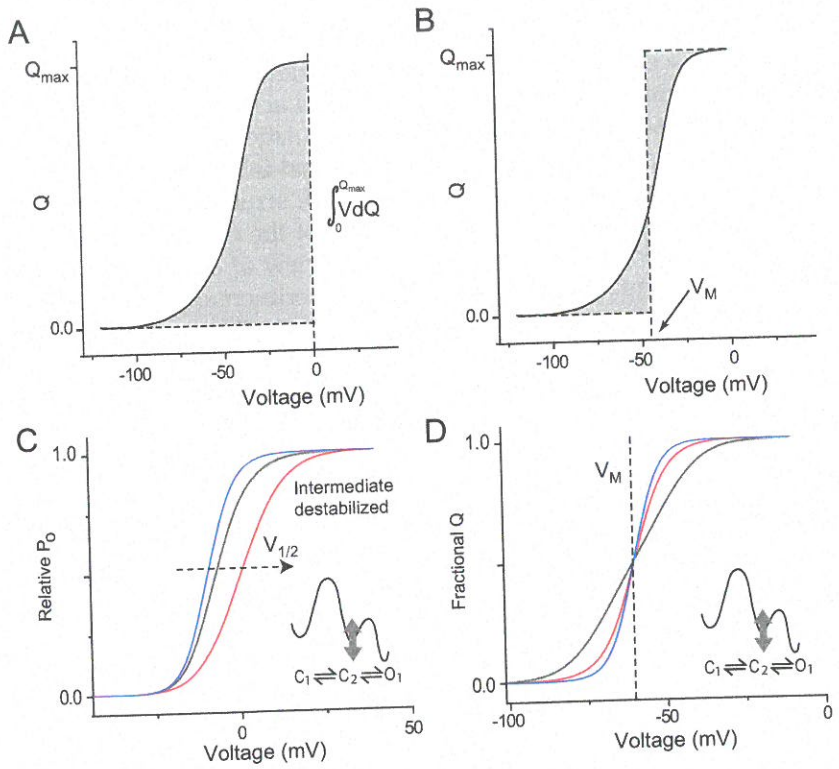

FIGURE 2.4
Model-free measurements of free energy of voltage-dependent activation. (A and B) A typical charge–voltage (QV) plot of a voltage-gated ion channel where the y-axis is the charge per channel and x-axis is the voltage. Q_{max} is the maximum charge per channel. The shaded area under the QV curve and ordinate axis (shown in A) represents the chemical components of the total free-energy change associated with voltage-dependent activation of the channel. The dashed line in (B) represents the median voltage axis (V_M), which is the voltage where the two shaded areas on either side of the V_M axes are equal. When this condition is satisfied, then the area under the curve depicted in (A) can be calculated by simply taking the product of Q_{max} and V_M. (C and D) A comparison of how the stabilities of intermediate states alter the P_O–V and QV curves. (C) shows P_O–V for a sequential model (inset). These curves were generated by changing the stability of the intermediate C_2 state, while keeping the net energy difference between the initial and final states of the system (C_1 and O_1, respectively) fixed. Fitting these data to a Boltzmann function and using the fit parameters $zFV_{1/2}$ to calculate the free energies will give three different values even though the net free energy remains unchanged. (D) QV plots with the same three state schemes as in (C). Changes in the stability of the intermediate state C_2 changes the shape of the QV curve but does not affect the value of V_M of activation. Thus, the parameter V_M is solely governed by the difference in the energy between the initial and final states of the system.

area between the QV curve and the Q (ordinate) axis, reflects the chemical component of the free-energy change, G_c. It can be shown that G_c is simply

$$\Delta G_C = Q_{max} F V_M \tag{2.20}$$

where V_M (median voltage for activation) is the voltage that divides the QV curves into two parts of equal areas (Figure 2.4b). The preceding free-energy relationship allows us to accurately and directly estimate the free-energy associated with channel gating without any prior knowledge of the underlying kinetic mechanisms (Figure 2.4c and 2.4d).

The ability to obtain accurate measurements of the free energy of channel gating makes it possible to use thermodynamic tricks to learn more about the molecular forces that determine structure. One such method is the generalized interaction energy analysis (GIA), which has been used to measure pairwise interaction energies between different sites or side chains (Chowdhury, Haehnel, and Chanda 2014). This method is based on the double mutant cycle analysis pioneered by Alan Fersht and his colleagues to study Barnase–Barstar interactions (Carter et al. 1984). Simply stated, the method involves comparing the free energies of the double mutations with linear summation of the free energies of the individual mutants. For instance, if we consider two sites, A and B, in an ion channel, the free energy of interaction between the two sites (ΔG_{A-B}) can be obtained by using the following equation:

$$\Delta G_{A-B} = \left(\Delta G_{WT} - \Delta G_{A}\right) - \left(\Delta G_{B} - \Delta G_{AB}\right) \tag{2.21}$$

ΔG_{A} and ΔG_{B} correspond to the free energy of gating of single mutants at the *A* and *B* positions. ΔG_{AB} and ΔG_{WT} are median voltage values for the *AB* double mutant and *WT* channel, respectively. If the sites are not interacting, the ΔG_{A-B} is zero otherwise and it corresponds to the net interaction energy between these sites. These methods have been recently used to map allosteric interaction pathways underlying voltage-dependent opening in voltage-gated potassium ion channels (Fernandez-Marino et al. 2018).

2.3 Biophysical Methods to Probe Voltage-Sensing Mechanisms

The advent of molecular cloning stimulated mechanistic thinking in terms of the underlying chemical structures and their role in ion channel function. In this section, we will briefly summarize the key biophysical approaches to study the mechanisms of voltage-dependent gating.

2.3.1 Gating Charge per Channel

To understand the mechanism of voltage sensing, it is necessary to first identity the voltage-sensing charges. This is akin to identifying what the ligand-binding site is in a ligand-gated ion channel. While in the VGICs, the positive-charged residues (arginines and lysines) in the S4 segment are likely to be the gating charges; there is no a priori reason to assume that these are the only voltage-sensing residues. Moreover, not all charged residues in the S4 segment may contribute to voltage sensing. Only if a mutation of a charged residue reduces the gating charge per channel, then that residue is considered a bona fide voltage sensor. As discussed earlier, gating charge per channel (Q_{max}) can be estimated by using the limiting slope method when the channel activation is completely sequential. A more general and direct method is to measure the total gating charge per cell and then independently determine the number of channels in that cell. In experiments on the Shaker potassium channel, the total number of channels per cell were estimated by either using a radioligand binding measurements or by noise analysis (see Chapter 8 for details on noise analysis) (Aggarwal and MacKinnon 1996; Seoh et al. 1996; Schoppa et al. 1992).

More recently, fluorescence from ion channels tagged with a fluorescent protein has been used to obtain a relative estimate of gating charge per channel (Gamal El-Din et al. 2008).

In these experiments, fluorescence-gating charge (F-Q) curves were generated by plotting the surface fluorescence with respect to gating currents for every cell. By comparing the slope of the F-Q plot of mutants with that of the wild-type channel, it is possible to obtain a relative estimate of the gating charge per channel for the mutants.

2.3.2 Substituted Cysteine Accessibility Method (SCAM)

One of the early approaches to probe conformational change in a voltage-gated ion channel is the substituted cysteine accessibility method (SCAM). In a membrane protein, each residue is either accessible to the surrounding water molecules or buried in the lipid bilayer or protein interior. Water-exposed cysteine side chains form ionized thiolate (RS–), which reacts a billion times faster with MTS derivatives than the nonionized thiol groups (RSH). Therefore, reactivity to MTS derivatives is a measure of water accessibility of a cysteine at a particular site and, depending on their location in the structure, changes in cysteine accessibility in response to a stimulus can be a probe of local conformation. Cysteine reactivity to MTS reagents is typically assayed by measuring the effect on this modification on channel function. Akabas and Karlin first developed this method to probe conformational changes in acetylcholine receptor (Akabas et al. 1992). Yang and Horn (1995) were the first to apply this approach on voltage-gated ion channel to show that the S4 voltage-sensing segment of a sodium channel moves in response to a change in membrane potential. Since then, SCAM has been widely adopted to probe conformational changes in various other ion channels, including in the Shaker potassium channel.

2.3.3 Voltage-Clamp Fluorometry (VCF)

Another approach to probe voltage-dependent conformational change is to introduce a fluorescent reporter at various sites in the ion channel. Fluorescence emission is highly sensitive to the local environment; solvent, pH, quenching groups and electric field can influence the emission spectra and intensity of the fluorescence signal. In voltage-clamp fluorometry (VCF), fluorescence measurements are carried out in voltage-clamp configuration that allows simultaneous tracking of function and structure. Unlike SCAM, VCF can also provide information about the kinetics of conformational change near the labeling site. Isacoff and colleagues were the first to implement this approach to measure voltage-induced conformational changes in the Shaker S4 segment (Mannuzzu, Moronne, and Isacoff 1996). Similar measurements on the S4 segments of the voltage-gated sodium channel revealed the roles of S4 of domain III and IV in sodium channel inactivation (Cha, Ruben, et al. 1999). Over the past two decades, VCF and a related PCF (patch-clamp fluorometry) have been powerful biophysical approaches to probe conformational dynamics and correlate it with the functional state of the channel (Zheng and Zagotta 2000). A more detailed review of this approach will be provided in Chapter 11.

2.3.4 Gating Pore Currents

Starace and Bezanilla discovered that the mutations of some of the charged residues to histidines made the Shaker potassium channel permeable to protons (Starace, Stefani, and Bezanilla 1997). They were able to demonstrate that the proton permeation pathway resides in the voltage-sensing domain (VSD) and that it is voltage-dependent. Subsequently, it was shown that neutralizing the S4 charges can elicit gating pore currents that are both voltage-dependent and can pass cations as large as guanidium ions (Tombola, Pathak,

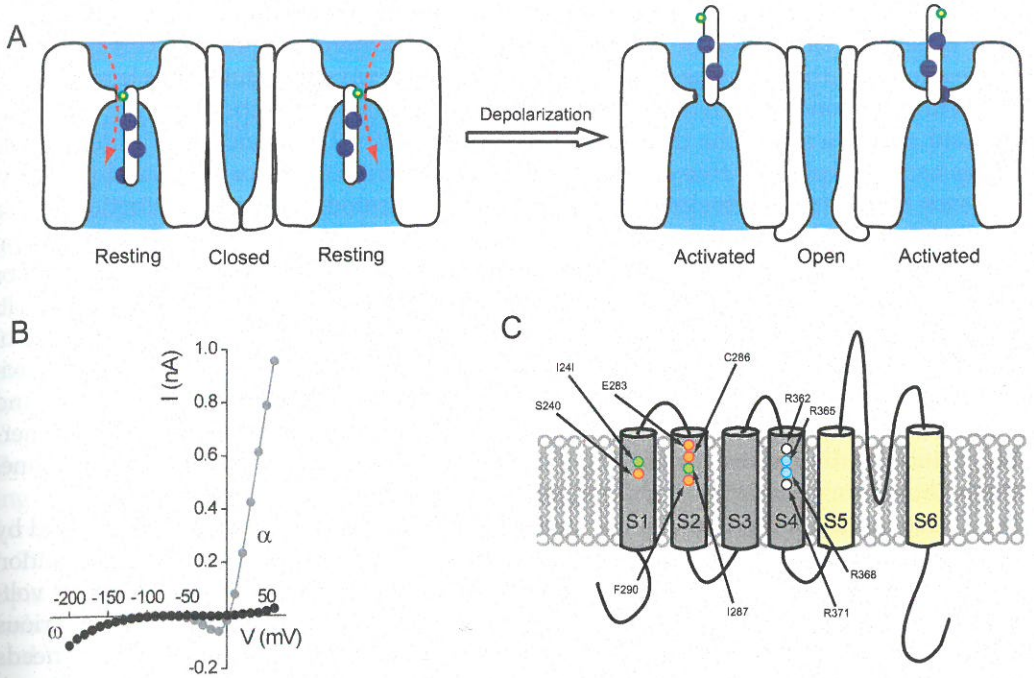

FIGURE 2.5
Gating pore currents. (A) At hyperpolarizing voltages, when the channel is closed and the voltage sensor is in resting conformation, the first gating charge is positioned near the gating septum, which separates the external and internal water-filled crevices in the voltage sensor. Mutation of this gating charge to a small/neutral amino acid allows small free cations in solution to sneak through the gating septum giving rise to gating pore currents. Activation of the voltage sensor by depolarization positions the last gating charge near the gating septum, thereby occluding flux through the gating pore pathway and making it state-dependent. (B) Current–voltage plots of the R1 mutant of the Shaker potassium channel in the absence and presence of Agitoxin. Agitoxin specifically blocks the flux of potassium ions through the principal pore (constituted by S6 helices) but does not inhibit the flux of the ions through the gating pore. (Data from Tambola et al. 2005.) (C) Sites in the Shaker potassium channel, which, upon mutation, give rise in state-dependent gating pore currents. (Adapted from Chanda and Bezanilla, Neuron 2008).

and Isacoff 2005). Gating pore currents are a consequence of a remarkable feature of the voltage-sensing domain wherein the electric field is focused over a very narrow region referred to as the gating septum, which separates the intracellular side from the extracellular side (Ahern and Horn 2004). In absence of charged S4 residues, ions and protons can sneak through the gating septum at a measurable rate that is detected as gating pore currents. These small currents can be detected only when the primary pore currents are abolished by a pore blocker or in the background of a nonconducting mutation. Depending on the position of the mutated residue, the gating pore currents are observed either in the activated state or in resting conformation. These voltage-dependent VSD currents become a very useful tool to monitor the conformational state of the voltage sensor (Figure 2.5).

2.3.5 Thermodynamic Mutant Cycle Analysis of Interaction Energies

Thermodynamic mutant cycle analysis is a widely used technique to determine interaction energies between two sites within a protein molecule or between two interacting molecules. Since energies are additive, a change in free energy due a double mutation should

correspond to the sum of the change in free energy due to each of the single mutations, unless these two sites interact. In that case, the nonadditive component corresponds to the free energy of the pairwise interaction between the two sites. Mutant cycle analysis is a powerful and conceptually straightforward tool to probe interaction energies, but it is important to be aware of the limitations of this approach. The principle of mutant cycle analysis can be applied to free energies and not to any functional or structural property. The reason being that the free energy of a system is a thermodynamic state function whose value does not depend on the path but only on the initial and the final states. Structural and functional parameters, by contrast, are path functions rather than state functions. For instance, consider the conductance-voltage curve, which is a functional property of a voltage-dependent ion channel but has been used as a surrogate to estimate the free energy of channel activity by fitting it to a single Boltzmann function under the two-state approximation (Zandany et al. 2008). For most ion channels, this approximation is not valid and the free-energy value calculated from G-V curves in such cases is dependent on the energetics of intermediate states and hence, it no longer represents the free energy of channel gating (Chowdhury, Haehnel, and Chanda 2014).

For voltage-gated ion channels, the free energy of channel gating can be obtained by measuring the charge-voltage curves and using the median voltage method (Equation 2.20). As described earlier, thermodynamic mutant cycle analysis based on median voltage-estimates (GIA) can be used to probe pairwise interaction energies between various residues and their contribution to channel gating. To apply this approach, one also needs to calculate the charge per channel. If the mutations do not involve charge residues, it can be assumed that the charge per channel is unchanged and use wild-type values. While this approach is broadly applicable to any voltage-gated ion channel, we should note that in many cases it is challenging to record gating currents due to lack of sufficient expression.

2.3.6 Structural Approaches

Structure-based approaches can provide molecular-level descriptions of the structural changes during the voltage-gating cycle and in recent decades have revolutionized our understanding of the mechanisms of voltage gating (Doyle et al. 1998; Long, Campbell, and Mackinnon 2005a). High-resolution structures set the stage for building detailed mechanistic models and designing new experiments to test these models. Developments in membrane protein crystallography and more recently cryo-EM technology has ushered in a resolution revolution in the field (Liao et al. 2013). Representatives of at least one member of every family of VGICs are now available. Structure of VGICs have been solved in multiple conformations representing various intermediates during the gating cycle (Clairfeuille et al. 2019; Guo et al. 2016; Shen et al. 2018; Shen et al. 2019; Long et al. 2007; Wisedchaisri et al. 2019). In some cases, the structures have no obvious correlate with any known functional state. This lack of correlation is not necessarily surprising because kinetic models are built on the principle of parsimony, and it is not possible to rule out more complex gating schemes that involve additional conformational states that may be captured in some studies but not others.

Voltage-clamp fluorometry can bridge some of the divide between the various structures and functional states (Tombola, Pathak, and Isacoff 2006; Cowgill and Chanda 2019). FRET and related methods provide subnanometer level descriptions of relative conformational changes during the gating cycle (Posson et al. 2005). The primary advantage of this approach is that these measurements are carried out in functional channels in a native

lipid environment. In some cases, it is possible to correlate specific conformational change with a kinetic transition or entry into a functional state.

2.3.7 Computational Approaches

Computational approaches have become increasingly important even though at present it is not possible to run molecular simulations that drive the channel through a complete gating cycle. In a technical tour de force, Shaw and his group used a special-purpose supercomputer to simulate the voltage-driven deactivation of a voltage-sensing potassium channel by applying extraordinarily large electric fields to hasten the process (Jensen et al. 2012). However, most academic labs have limited access to these resources and much of the effort in the field has focused on enhanced sampling methods to bridge molecular dynamics (few microseconds) and experimental (tens of milliseconds and beyond) time scales. Computational approaches have been used to identify the possible interaction sites during the gating process and also track how conformational energy is transmitted from the sensing or modulator domain to pore gates by using allosteric network analysis (Kasimova, Lindahl, and Delemotte 2018).

To simulate voltage-dependent gating, it is necessary to apply an electric field across the lipid bilayer. Computationally there are two ways this can be achieved. In one case, charge imbalance is created by introducing ionic gradients across the lipid bilayer (Sachs, Crozier, and Woolf 2004). While the forces experienced by the atoms in the transmembrane regions are more realistic, given the small size of the periodic cell even a single charge translocation can significantly alter the membrane potential. An alternate approach involves the application of a uniform electric field throughout the entire periodic cell, oriented such that it is perpendicular to the plane of the membrane (Roux 1997). In bulk solution, the ions reorient to neutralize most of the electric field such that the steepest gradient is over the low dielectric membrane. A detailed discussion of the various computational approaches will be covered in Chapter15.

2.4 Voltage-Sensor Motions

The first structures of voltage-sensing ion channels revealed that the voltage-sensing domain consisting of S1–S4 helix is a four-helix bundle domain where the charged S4 residues either interact with water molecules inside the crevices or with lipid headgroups (Long, Campbell, and Mackinnon 2005a; Long et al. 2007). Much of the early studies characterizing the mechanism of voltage sensing were carried out on the Kv channels, but more recently high-resolution structures of two-pore channels and sodium channels have provided new insights (Guo et al. 2016; Shen et al. 2019; Xu et al. 2019). Here, we will present some of the key features of the voltage-sensing domain and emerging views regarding the movements of the voltage sensor. First, the voltage-sensing domain forms a water-filled permeation pathway for movement of voltage-sensing charges (Krepkiy, Gawrisch, and Swartz 2012). However, the permeation pathway is not contiguous but interrupted by the charge transfer center, which is capped on the extracellular side by conserved phenylalanine and negatively charged residues on the intracellular side (Tao et al. 2010). Note that the charge transfer center has also been referred to as the gating septum by researchers in the field. The charge transfer center facilitates the movement of the voltage-sensing charges

between the extracellular and intracellular water-filled crevices. These structural features ensure that the electric field is focused within the voltage-sensing domain and most of that drop occurs over a distance of 4 Å (Ahern and Horn 2004; Starace and Bezanilla 2004) (see Box 2.1). The first four arginine residues on the S4 helix carry most of the gating charges (Seoh et al. 1996; Aggarwal and MacKinnon 1996). Some of these charges are stabilized by interaction with acidic residues in other helices, but the first charge has been shown to interact with acidic headgroups of the surrounding lipids (Tiwari-Woodruff et al. 1997; Long et al. 2007; Xu, Ramu, and Lu 2008). The composition of the surrounding lipid can have a significant influence on the voltage dependence of gating (Figure 2.6).

The nature and extent of the voltage-sensing motion underlying the activation of depolarization-activated channels have been extensively investigated (Swartz 2008; Bezanilla 2008; Tombola, Pathak, and Isacoff 2006). Before the high-resolution structures became available, there were two competing models of voltage sensing. In the transporter model, the water-filled crevices in the voltage-sensing domain were envisioned to undergo a conformational switch from an outside-facing conformation to an inside-facing state upon membrane hyperpolarization (Starace and Bezanilla 2004; Cha, Snyder, et al. 1999). The

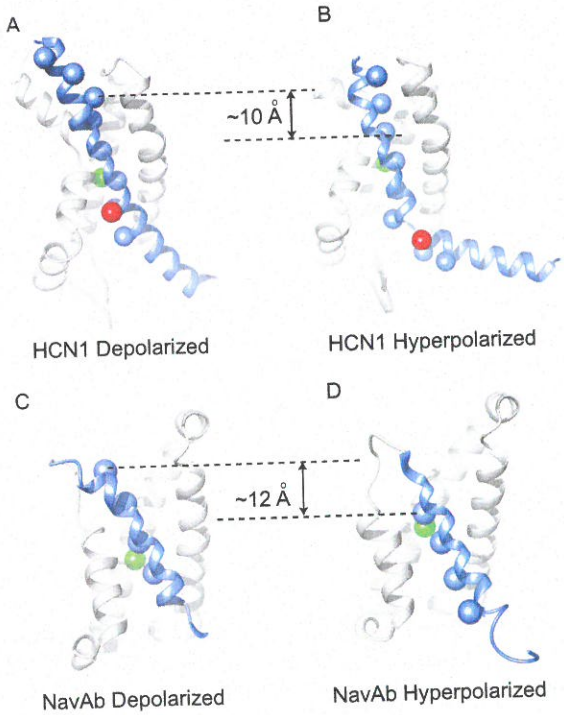

FIGURE 2.6
Structures of the voltage sensors of hyperpolarization- and depolarization-gated channels in activated and resting conformations. (A and B) The structure of the voltage sensor of the HCN1 channel in a depolarized state (A) and in a metal-bridge-locked hyperpolarized state (B). The S4 helix is in blue, while S1, S2, S3 are in light gray. The blue spheres represent the charged residues on the S4 segment and the red sphere indicates a conserved Serine residue that facilitates the bending of the S4 helix between the two conformations. The conserved phenylalanine residue representing the gating charge transfer center is shown as a green sphere. There is a vertical displacement of ~10Å in the S4 segment between the two conformations. (C and D) The structure of the voltage sensor of the NavAb channel in an activated conformation (C) and in a metal-bridge-locked resting state (D). The color scheme is the same as before. There is a vertical displacement of ~11.5Å in the S4 segment between the two conformations.

proposed movement of the S4 segment is limited in this model and the charge transport occurs due to a change in the position of the gating septum. The alternate model, by contrast, posits that the S4 helix undergoes a helical screw translational motion to transfer gating charges from the outside to inside past the gating septum (Yang, George, and Horn 1996; Baker et al. 1998). Most voltage-sensing domains are in activated conformation at 0 mV and since the structures are solved in absence of an electric field, voltage-sensing domains in these structures are only captured in activated conformation. By chemically trapping the voltage sensor in down conformation, researchers have successfully solved a number of structures of the voltage-sensing domain in resting state (Guo et al. 2016; She et al. 2018; Shen et al. 2018; Clairfeuille et al. 2019; Xu et al. 2019; Shen et al. 2019; Wisedchaisri et al. 2019). These resting-state structures of the voltage-sensing domain in two-pore channels and sodium channels are in general consistent with helical screw motion in the voltage-sensor domain.

For many years, it was implicitly assumed that similar voltage-sensing motions occur in the hyperpolarization-activated ion channels, but the primary difference between them and their depolarization-activated channels is the inversion of the coupling such that the pore is open when the voltage sensor is in down conformation (Mannikko, Elinder, and Larsson 2002; Latorre et al. 2003). Structural studies reveal the voltage-sensing S4 helix in hyperpolarization-activated channels is at least one helical turn longer (Lee and MacKinnon 2017). Unexpectedly, when this S4 helix moves to a down position, it breaks in the middle with the lower half forming a structure that resembles the S4–S5 linker in domain-swapped channels (Lee and MacKinnon 2019). Functional measurements show that the polarity of residue at the breakpoint is a critical determinant of the direction of rectification; hydrophobic residues at that position favor depolarization activation, whereas the hydrophilic residues favor hyperpolarization activation (Kasimova et al. 2019). Sequence analysis of the protein database shows that the polarity of the amino acids residues is also directly correlated with the helix-breaking propensity in membrane proteins. While the generality of these concepts remains to be established, the emerging view is that the voltage-sensor motion in the hyperpolarization-activated channels involves an additional conformational switch that it not observed in their depolarization-activated counterparts.

2.5 Coupling of Voltage-Sensor Motion to Pore Opening

One of the key questions in the field is: How are the voltage-sensor motions coupled to opening and closing of the pore gates in the VGIC superfamily? Before we get into that, let us take a moment to consider the overall structure of the voltage-sensing domain and pore in a functional VGIC. They are either arranged in a domain-swapped or non-domain-swapped architecture. The main characteristic of domain-swapped architecture is that the VSD is juxtaposed to the neighboring pore domain and the structured S4–S5 linker connects these two domains, whereas in the non-domain-swapped channels, the VSD is placed right next to its own pore domain and is connected to its pore domain by a short unstructured linker (Long, Campbell, and Mackinnon 2005a; Whicher and MacKinnon 2016). Thus, there are two possible pathways for communication between the voltage sensor and the pore: one involving the structured S4–S5 linker and the other via the transmembrane interfaces between the S4 and S5 segments. For historical reasons, the allosteric pathways involving the structured S4–S5 linker are delineated as canonical pathways,

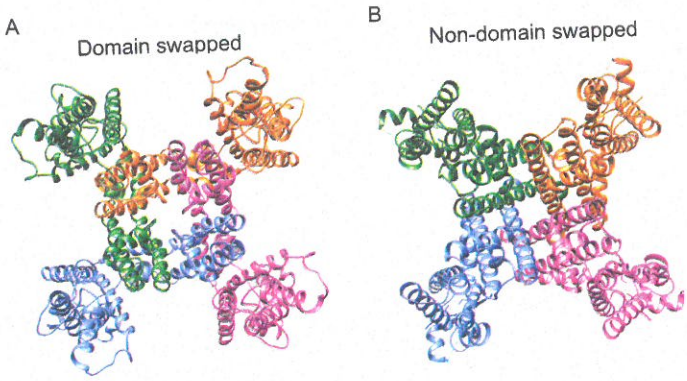

FIGURE 2.7
Arrangements of the voltage sensor and pore in VGICs. (A) Top view of the Kv1.2/2.1 paddle chimera in lipid nanodiscs showing a domain-swapped arrangement of the VSD and the pore. The four subunits are colored differently. The voltage sensor of a subunit forms intimate contacts with the pore domain (specifically the S5 helix) of the neighboring domain in a clockwise direction. (B) Top view of the HCN1 channel showing a non-domain-swapped arrangement of the VSD and the pore. In this case, each VSD is proximal to the pore domain of its own subunit.

whereas those involving direct communication between the membrane spanning S4 and S5 segments are loosely referred to as noncanonical pathways (Figure 2.7).

One of the strongest evidence regarding the role of the S4–S5 linker in the voltage-sensor pore coupling came from studies by Lu and coworkers who discovered that the bacterial potassium channel can be made voltage-dependent by fusing the voltage-sensing domain of the Shaker potassium channel (Lu, Klem, and Ramu 2001). They also found that the S4–S5 linker and distal parts of the S6 are crucial for conferring voltage dependence. Subsequent studies using site-directed mutagenesis and other approaches further supported the crucial role of the linker region and distal part of S6 in electromechanical coupling (Lu, Klem, and Ramu 2002). The structures of the domain-swapped voltage-gated ion channels show that the S4–S5 linker is a short helix that sits parallel to the membrane and is also in direct contact with the distal region of the S6 segment. One can envision a physical mechanism wherein a movement of the S4 voltage-sensing helix will be transmitted via the linker to the S6 helix that forms part of the pore gates (Long, Campbell, and Mackinnon 2005b).

A characteristic structural feature of the non-domain-swapped channels is that the S4–S5 linker helix is replaced by a short unstructured loop (Whicher and MacKinnon 2016). Insertion of a break or even deletion of this loop does not appear to have a significant effect on voltage gating (Lorinczi et al. 2015; Flynn and Zagotta 2018). Even in the Shaker channel as well as in the KCNQ channels, it has been shown that the interactions between S4 and S5 helices are involved in mediating voltage-sensor pore coupling (Li-Smerin, Hackos, and Swartz 2000; Fernandez-Marino et al. 2018; Hou et al. 2017, 2020). These interaction pathways mediated by direct interactions between the S4 and S5 helices are referred to as the noncanonical coupling pathway and are likely to be important in electromechanical coupling of non-domain-swapped voltage-gated ion channels.

Despite much progress in the past decade, our understanding of the mechanisms of electromechanical coupling remains far from complete. Although multiple structures of depolarization-activated ion channels in the resting and activated conformations are now available, many details regarding the mechanisms of electromechanical coupling remain to be worked (see Box 2.2). For instance, we do not have a clear sense as to the relative

energetic contributions of the two major electromechanical coupling pathways in VGICs. Further investigation of other members of the VGIC family beyond the handful of prototypical channels will help build a more comprehensive view of the mechanisms of electromechanical coupling. Finally, compared to the depolarization-activated ion channels, our understanding of the forces and physical mechanisms of EM coupling in hyperpolarization-activated channels remains very limited.

2.6 Concluding Remarks

It is becoming increasingly evident that other processes involving membrane signaling also exhibit voltage dependence, which in some instances have physiological significance. Many G protein-coupled receptors (GPCRs), which are primarily involved in chemical signaling, are also regulated by voltage, which is likely to be mediated via sodium ion binding pocket deep in the transmembrane regions. While the voltage-sensing mechanisms discussed in this chapter focused on the VGICs, many of these principles and approaches are broadly applicable to many other membrane proteins and voltage-sensing molecules in living cells.

Acknowledgments

We are grateful to the National Institutes of Health for continuously funding our research. Due to space constraints, we were unable to cover many interesting aspects of voltage gating, but we hope that some of them will be introduced in more specialized sections of this book series. We also owe a debt to the giants in the field whose original writings inspired some of the material in this chapter.

Suggested Readings

This chapter includes additional bibliographical references hosted only online as indicated by citations in blue color font in the text. Please visit https://www.routledge.com/9780367538163 to access the additional references for this chapter, found under "Support Material" at the bottom of the page.

Aggarwal, S. K., and R. MacKinnon. 1996. "Contribution of the S4 segment to gating charge in the Shaker K+ channel." *Neuron* 16 (6):1169–77.

Almers, W. 1978. "Gating currents and charge movements in excitable membranes." *Rev Physiol Biochem Pharmacol* 82:96–190.

Armstrong, C. M. 1981. "Sodium channels and gating currents." *Physiol Rev* 61 (3):644–83. doi:10.1152/physrev.1981.61.3.644.

Armstrong, C. M., and F. Bezanilla. 1973. "Currents related to movement of the gating particles of the sodium channels." *Nature* 242 (5398):459–61.

Bezanilla, F. 2000. "The voltage sensor in voltage-dependent ion channels." *Physiol Rev* 80 (2):555–92. doi:10.1152/physrev.2000.80.2.555.

Carter, P. J., G. Winter, A. J. Wilkinson, and A. R. Fersht. 1984. "The use of double mutants to detect structural changes in the active site of the tyrosyl-tRNA synthetase (Bacillus stearothermophilus)." *Cell* 38 (3):835–40. doi:10.1016/0092-8674(84)90278-2.

Chanda, B., and F. Bezanilla. 2002. "Tracking voltage-dependent conformational changes in skeletal muscle sodium channel during activation." *J Gen Physiol* 120 (5):629–45. doi:10.1085/jgp.20028679.

Chanda, B., and F. Bezanilla. 2008. "A common pathway for charge transport through voltage-sensing domains." *Neuron* 57 (3):345–51. doi:10.1016/j.neuron.2008.01.015.

Chowdhury, S., and B. Chanda. 2012. "Estimating the voltage-dependent free energy change of ion channels using the median voltage for activation." *J Gen Physiol* 139 (1):3–17. doi:10.1085/jgp.201110722.

Chowdhury, S., B. M. Haehnel, and B. Chanda. 2014. "A self-consistent approach for determining pairwise interactions that underlie channel activation." *J Gen Physiol* 144 (5):441–55. doi:10.1085/jgp.201411184.

Guo, J., W. Zeng, Q. Chen, C. Lee, L. Chen, Y. Yang, C. Cang, D. Ren, and Y. Jiang. 2016. "Structure of the voltage-gated two-pore channel TPC1 from Arabidopsis thaliana." *Nature* 531 (7593):196–201. doi:10.1038/nature16446.

Hagiwara, S. 1966. "Membrane properties of the barnacle muscle fiber." *Ann N Y Acad Sci* 137 (2):1015–24.

Hamill, O. P., A. Marty, E. Neher, B. Sakmann, and F. J. Sigworth. 1981. "Improved patch-clamp techniques for high-resolution current recording from cells and cell-free membrane patches." *Pflugers Arch* 391 (2):85–100. doi:10.1007/BF00656997.

Hodgkin, A. L., and A. F. Huxley. 1952e. "A quantitative description of membrane current and its application to conduction and excitation in nerve." *J Physiol* 117 (4):500–44.

Humphries, J., L. Xiong, J. Liu, A. Prindle, F. Yuan, H. A. Arjes, L. Tsimring, and G. M. Suel. 2017. "Species-independent attraction to biofilms through electrical signaling." *Cell* 168 (1–2):200–9 e12. doi:10.1016/j.cell.2016.12.014.

Islas, L. D., and F. J. Sigworth. 2001. "Electrostatics and the gating pore of Shaker potassium channels." *J Gen Physiol* 117 (1):69–89.

Jensen, M. O., V. Jogini, D. W. Borhani, A. E. Leffler, R. O. Dror, and D. E. Shaw. 2012. "Mechanism of voltage gating in potassium channels." *Science* 336 (6078):229–33. doi:10.1126/science.1216533.

Kasimova, M. A., D. Tewari, J. B. Cowgill, W. C. Ursuleaz, J. L. Lin, L. Delemotte, and B. Chanda. 2019. "Helix breaking transition in the S4 of HCN channel is critical for hyperpolarization-dependent gating." *Elife* 8. doi:10.7554/eLife.53400.

Lee, C. H., and R. MacKinnon. 2017. "Structures of the human HCN1 hyperpolarization-activated channel." *Cell* 168 (1–2):111–20 e11. doi:10.1016/j.cell.2016.12.023.

Liao, M., E. Cao, D. Julius, and Y. Cheng. 2013. "Structure of the TRPV1 ion channel determined by electron cryo-microscopy." *Nature* 504 (7478):107–12. doi:10.1038/nature12822.

Long, S. B., E. B. Campbell, and R. Mackinnon. 2005a. "Crystal structure of a mammalian voltage-dependent Shaker family K+ channel." *Science* 309 (5736):897–903. doi:10.1126/science.1116269.

Lorinczi, E., J. C. Gomez-Posada, P. de la Pena, A. P. Tomczak, J. Fernandez-Trillo, U. Leipscher, W. Stuhmer, F. Barros, and L. A. Pardo. 2015. "Voltage-dependent gating of KCNH potassium channels lacking a covalent link between voltage-sensing and pore domains." *Nat Commun* 6:6672. doi:10.1038/ncomms7672.

Lu, Z., A. M. Klem, and Y. Ramu. 2001. "Ion conduction pore is conserved among potassium channels." *Nature* 413 (6858):809–13. doi:10.1038/35101535.

Mannikko, R., F. Elinder, and H. P. Larsson. 2002. "Voltage-sensing mechanism is conserved among ion channels gated by opposite voltages." *Nature* 419 (6909):837–41. doi:10.1038/nature01038.

Mannuzzu, L. M., M. M. Moronne, and E. Y. Isacoff. 1996. "Direct physical measure of conformational rearrangement underlying potassium channel gating." *Science* 271 (5246):213–16. doi:10.1126/science.271.5246.213.

Seoh, S. A., D. Sigg, D. M. Papazian, and F. Bezanilla. 1996. "Voltage-sensing residues in the S2 and S4 segments of the Shaker K+ channel." *Neuron* 16 (6):1159–67.

Starace, D. M., E. Stefani, and F. Bezanilla. 1997. "Voltage-dependent proton transport by the voltage sensor of the Shaker K+ channel." *Neuron* 19 (6):1319–27.

Xu, Y., Y. Ramu, and Z. Lu. 2008. "Removal of phospho-head groups of membrane lipids immobilizes voltage sensors of K+ channels." *Nature* 451 (7180):826–9. doi:10.1038/nature06618.

Yang, N., and R. Horn. 1995. "Evidence for voltage-dependent S4 movement in sodium channels." *Neuron* 15 (1):213–18.

Zagotta, W. N., T. Hoshi, and R. W. Aldrich. 1994. "Shaker potassium channel gating. III: evaluation of kinetic models for activation." *J Gen Physiol* 103 (2):321–62.

Zheng, J., and W. N. Zagotta. 2000. "Gating rearrangements in cyclic nucleotide-gated channels revealed by patch-clamp fluorometry." *Neuron* 28 (2):369–74. doi:10.1016/s0896-6273(00)00117-3.